Taylor & Francis
Taylor & Francis Group

ANALYSIS OF RADIATIVE EFFECT UNDER LOCAL THERMAL NON-EQUILIBRIUM CONDITIONS IN POROUS MEDIA-APPLICATION TO A SOLAR AIR RECEIVER

P. Wang[1,2], K. Vafai[2], and D. Y. Liu[1]

[1]*Department of Water Conservancy and Hydropower Engineering, Hohai University, Nanjing, P.R. China*

[2]*Department of Mechanical Engineering, University of California, Riverside, California, USA*

The effect of thermal radiation within a porous medium while incorporating local thermal nonequilibrium (LTNE) is investigated in this work, with specific application to solar air receivers. It is shown that the radiation effect is significant. The temperature distributions for both solid and fluid phases are affected by conduction-radiation parameter N, the ratio of solid to fluid phase conductivities ζ, and the interphase convection parameter H. The limiting interactions between conduction and thermal radiation incorporating convection are revealed. The impact of conduction and convection versus radiation is systematically analyzed in this work and displayed through a number of contour maps.

1. INTRODUCTION

Porous media is widely utilized in many modern industrial applications involving heat transfer processes, such as solar thermal utilization, nuclear waste repository, heat pipes, combustion, heat transfer enhancement, etc. [1]. One area of utilization is the receiver [2] of a central receiver system (CRS) in solar thermal power plants due to the unique feature of silicon carbide (SiC) foam ceramic, such as large specific area, high conductivity, and thermal shock resistance. In CRS, the porous material receives the concentrated sunlight from the heliostat field and heats up the pumped inlet air by convection and radiation.

Convective heat transfer processes in porous media, as well as the local thermal nonequilibrium model incorporating the temperature difference between solid and fluid phase has been discussed in the literature [3–5]. Variants within the porous media transport models, including LTNE effects, has been analyzed by Amiri and Vafai [6–8], and the effects of different boundary conditions were analyzed by Yang and Vafai [9, 10], and Alazmi and Vafai [11]. Thermal radiation behavior in packed

NOMENCLATURE

c_p	specific heat of fluid at constant pressure, [J kg^{-1} K^{-1}]	α_{sf}	specific surface area of the porous medium, [m^{-1}]
F	inertial coefficient	ε	emissivity
d_p	pore diameter, [m]	φ	porosity
H	interphase convection parameter	λ	thermal conductivity/wave length, [W m^{-1} K^{-1}]
I	direct normal solar irradiance, [W m^{-2}]	μ	dynamic viscosity, [kg m^{-1} s^{-1}]
h_{sf}	fluid-to-solid heat transfer coefficient, [W m^{-2} K]	β	extinction coefficient, [m^{-1}]
K	permeability, [m^2]	σ	Stefan-Boltzmann constant
L	thickness of a porous medium, [m]	θ	dimensionless temperature
N_w	conduction-radiation parameter for jump coefficient	ζ	ratio of solid to fluid thermal conductivities
N	conduction-radiation parameter	ρ	density, [kg m^{-3}]
N_0	conduction-radiation parameter at boundary	ψ	jump coefficient
Nu	Nusselt number	**Subscripts**	
P	pressure, [Pa]	a	average
Pe	Peclet number	c	convective
Pr	Prandtl number	e	effective/environment
q_{in}	heat flux, [W/m^{-2}]	f	fluid phase
q_{loss}	radiation heat loss, [W/m^{-2}]	g	glass tube
Q	dimensionless incident heat flux	i	inlet
R_r	ratio of radiation to conduction heat flux	l	local
Re	Reynolds number	m	mean value
T	temperature, [K]	o	outlet
u	velocity, [m/s]	r	radiative
V	velocity vector [m s^{-1}]	ref	reference
		s	solid phase
		w	wall

and fluidized beds should be taken into account when dealing with high temperatures [12–14]. In this work, we need to utilize the governing equations which incorporate convection coupled with thermal radiation in porous media. The impact of radiation on conductive heat transfer in a packed bed and an open cell structure has been analyzed by Singh and Kaviany [15, 16] and Zhao et al. [17, 18], respectively. On the other hand, the radiative properties of porous structures have been obtained by Hendricks et al. [19, 20] and Baillis et al. [21, 22].

The heat transfer characteristics affected by air velocity, porosity, pore diameter and thickness in an air receiver was numerically analyzed by Bai et al. [23] and Xu et al. [24], and later validated by Wu et al. [25]. Some experimental and numerical investigations has been carried out to analyze the heat transfer efficiency [26], flow stability [27, 28] of the receiver, and the convective heat transfer coefficient of some typical materials with a porous structure [29, 30]. When the temperature of the solid phase is high, the effect of radiation on the temperature distribution should be taken into account simultaneously with conduction and convection processes. Not much attention has been devoted to incorporate these processes for volumetric air receivers. Hence, the purpose of this study is to understand the role of the thermal radiation on convective heat transfer in porous media specifically for these types of

devices. In this work, the temperature fields for the solid matrix and fluid phases will be analyzed while incorporating the local thermal non-equilibrium along with the diffusion approximation. The effect of conduction-radiation parameter N, ratio of solid to fluid conductivities ζ, and the interphase convection parameter H will be discussed, respectively. Furthermore, the limiting interactions incorporating conduction, convection and thermal radiation will be discussed. Finally, the contour maps for Nusselt numbers for a wide range of variations in the governing parameters, i.e., the conduction-radiation parameter, N, the ratio of solid to fluid conductivities, ζ and the interphase convection parameter, H will be systematically analyzed.

2. MODEL DESCRIPTION

2.1. Physical Model and Assumptions

Two types of air receivers are usually considered. One type has a closed cavity cooled by pressurized air. The advantage of this type is the attainment of higher temperatures with lesser radiation losses. However, the secondary reflector and glass window make it quite difficult to maintain this process. The second type, referred to as open-loop volumetric receiver is usually composed of many small modules and the concentrated flux is imposed on the receiver's surface which is cooled directly by the pumped air. Figure 1 shows the schematic structure of a SiC ceramic foam air receiver. As can be seen the receiver's surface area (y direction) is much larger than its thickness (x direction). As such a one dimensional approximation in the direction of the thickness is invoked. We will also assume that the solid matrix is homogeneous and isotropic, and the variations of the thermal properties of solid and fluid phases are neglected. Furthermore, the flow is considered to be steady and fully developed.

2.2. Mathematical Model

2.2.1. Governing equations. The governing equations incorporating the LTNE model and local volume average method are given in Eqs. (1)–(4) [3–11].

(a)   (b)
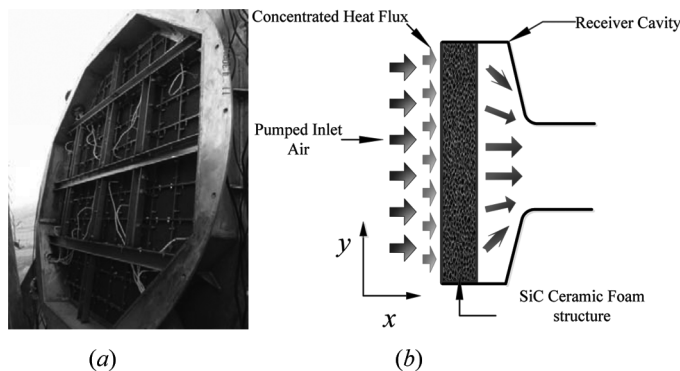
Figure 1. (a) Back of 1 MW air receiver test module in Beijing, and (b) schematic of the SiC ceramic foams air receiver.

Continuum equation

$$\nabla \cdot \langle V \rangle = 0 \tag{1}$$

Momentum equation

$$\frac{\rho_f}{\varphi} \langle (V \cdot \nabla) V \rangle = \frac{\mu_f}{\varphi} \nabla^2 \langle V \rangle - \nabla \langle P \rangle^f - \frac{\mu_f}{K} \langle V \rangle - \frac{\rho_f F \varphi}{\sqrt{K}} [\langle V \rangle \cdot \langle V \rangle] \mathbf{J} \tag{2}$$

Energy equations for the fluid and solid phases

$$(\rho c_p)_f \langle V \rangle \cdot \nabla \langle T_f \rangle = \nabla (\lambda_{fe} \cdot \nabla \langle T_f \rangle) + h_{sf} a_{sf} (\langle T_s \rangle - \langle T_f \rangle) \tag{3}$$

$$0 = \nabla \cdot (\lambda_{se} \cdot \nabla \langle T_s \rangle - q_r) - h_{sf} a_{sf} (\langle T_s \rangle - \langle T_f \rangle) \tag{4}$$

where $\langle P \rangle^f$ is the gauge pressure and the local volume average of a quantity Φ can be defined as $\langle \Phi \rangle \equiv \frac{1}{V_f} \int_{V_f} \Phi dV$, and J is a unit vector oriented along the velocity vector.

2.2.2. Radiation transfer. For most porous media utilized in industry, the ratio of the minimum dimension L to pore diameter d_p is substantially larger than 10, and the ratio of d_p to the wavelength λ is also large enough to be treated as a continuum [1]. The optical thickness τ is defined as follows.

$$\tau = \beta L \tag{5}$$

Where β is the extinction coefficient. For the SiC foam material used in the air receiver, τ is much larger than 10; consequently, the diffusion approximation [14, 31] will be applied to address the radiation transfer since the porous matrix can be considered to be optically thick. Here, we assume isotropic scattering and absorbing over the entire wave length band. As such the radiative flux can be expressed as follows.

$$q_r = -\frac{16\sigma(\langle T_s \rangle)^3}{3\beta} \nabla \langle T_s \rangle \tag{6}$$

Using Eq. (6) in Eq. (4) the energy equation for the solid phase can be presented as follows.

$$0 = \nabla \left(\left(\frac{16\sigma \langle T_s \rangle^3}{3\beta} + \lambda_{se} \right) \cdot \nabla \langle T_s \rangle \right) - h_{sf} a_{sf} (\langle T_s \rangle - \langle T_f \rangle) \tag{7}$$

2.2.3. Boundary conditions. The incident radiation flux q_{in} which is concentrated by a heliostat field, can be presented by the following.

$$q_{in} = 1 \, \mathrm{M \, W/m^2} \tag{8}$$

The heat flux at the boundary of the solid phase is considered as a surface phenomenon since we have an optically thick medium. Radiation heat loss between the receiver's surface and environment can be represented by the following.

$$q_{loss} = \sigma\varepsilon\left(\langle T_{s,in}\rangle^4 - \langle T_e\rangle^4\right) \tag{9}$$

The temperature of the inlet fluid, $T_{f,in}$ is the same as the environment temperature T_e, which is taken as follows.

$$T_{f,in} = T_e = 300\,K \tag{10}$$

When using the diffusion approximation when only the radiation process is taken into account, a jump boundary condition is usually utilized to connect the local radiative flux and emissive power gradient in the medium near the bounding surface [31]. For combined conduction-radiation, a similar concept is introduced: the jump boundary condition is given in terms of the jump coefficient ψ, which is a function of the conduction-radiation parameter N_w [32, 33].

$$\Psi(N_w) = \frac{\sigma\left(\langle T_w\rangle^4 - \langle T_{s(x\to 0)}\rangle^4\right)}{q_{r,w}} \tag{11}$$

Where the conduction-radiation parameter N_w can be expressed as follows.

$$N_w = \lambda_{se}\beta\big/4\sigma\langle T_w\rangle^3 \tag{12}$$

Meanwhile, the radiative flux $q_{r,w}$ under diffusion assumption can be expressed as follows.

$$q_{r,w} = -\frac{16\sigma\langle T_w\rangle^3}{3\beta}\frac{d\langle T_s\rangle}{dx}\bigg|_w = \frac{q_{in}}{3\beta\big/\left(16\sigma\big/3\beta + \lambda_{se}\big/\langle T_w\rangle^3\right)} \tag{13}$$

Combing the expression of the $q_{r,w}$, i.e., Eqs. (11) and (13). After linearizing it can be represented as follows.

$$\frac{4\Psi}{3}q_{in} = \frac{4\sigma}{3}\left(\langle T_w\rangle^4 - \langle T_{s(x\to 0)}\rangle^4\right) + \lambda_{se}\beta\left(\langle T_w\rangle - \langle T_{s(x\to 0)}\rangle\right) \tag{14}$$

For the outlet boundary, an adiabatic boundary condition is used as follows.

$$\frac{\partial\langle T_s\rangle}{\partial x} = 0 \tag{15}$$

$$\frac{\partial\langle T_f\rangle}{\partial x} = 0 \tag{16}$$

2.2.4. Normalization. The governing equations are nondimensionalized by introducing dimensionless variables. As such, the nondimensionalized energy equations for the fluid and solid phase can be represented as follows.

$$\text{Pe}\frac{\partial \theta_f}{\partial X} = \frac{\partial^2 \theta_f}{\partial X^2} + H(\theta_f - \theta_s) \tag{17}$$

$$0 = \frac{\partial}{\partial X}\left((N\theta_s^3 + \xi)\frac{\partial \theta_s}{\partial X}\right) + H(\theta_f - \theta_s) \tag{18}$$

Where,

$$N = \frac{16\sigma T_{ref}^3}{3\beta\lambda_{fe}}, \; N_0 = \frac{\varepsilon\sigma L T_{ref}^3}{\lambda_{fe}}, \; Q = \frac{qL}{T_{ref}\lambda_{fe}}, \; \zeta = \frac{\lambda_{se}}{\lambda_{fe}}, \; X = \frac{x}{L}$$

$$H = \frac{h_{sf}\alpha_{sf}L^2}{\lambda_{fe}}, \text{Re} = \frac{\rho uL}{\mu}, \text{Pr} = \frac{c_p\mu}{\lambda_{fe}}, \text{Pe} = \text{RePr}, \; T_{ref} = T_e,$$

$$\theta_s = \frac{T_s}{T_{ref}}, \; \theta_f = \frac{T_f}{T_{ref}}, \; \theta_e = 1$$

The boundary conditions, including Eq. (14), in dimensionless form can be represented as follows.

B.C.1: $X = 0$:

$$\theta_f = 1 \tag{19}$$

$$0 = -(N\theta_s^3 + 1)\frac{\partial \theta_s}{\partial X} + N_0(\theta_s^4 - \theta_e^4) - Q \tag{20}$$

$$\Psi(Q - N_0(\theta_w^4 - \theta_e^4)) = N_0\left(\theta_w^4 - \theta_{s(X\to 0)}^4\right) + \frac{3\xi\tau}{4}\left(\theta_w - \theta_{s(X\to 0)}\right) \tag{21}$$

B.C.2: $X = X_L$:

$$\frac{\partial \theta_f}{\partial X} = \frac{\partial \theta_s}{\partial X} = 0 \tag{22}$$

3. NUMERICAL PROCEDURE

Using a finite volume method, Eqs. (17)–(22) are discretized using a SIMPLE algorithm [34]. The discretization scheme, is based on a uniform grid set up and a cell centered scheme, as shown in Figure 2. Furthermore, first order upwind differencing method is employed to discretize the convective terms. The convergence is considered to have been reached when the relative variation of temperature between
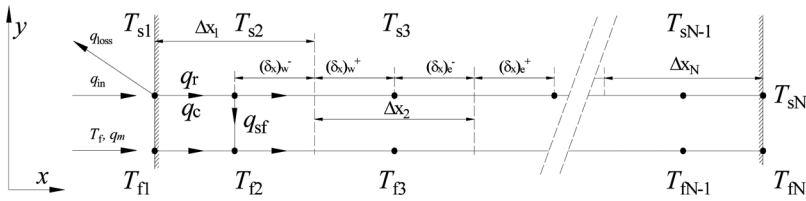
Figure 2. Grid system using the cell centered scheme finite volume method.

Table 1. Typical grid independence study performed in our investigation: $N = 1$, $H = 10^5$, $Pe = 10^4$, $\zeta = 10^3$

N_g	$Nu_{f,a}$	$Nu_{sc,a}$	$Nu_{sr,a}$	$\theta_{f,a}$	$\theta_{s,a}$
50	0.825785	0.284531	0.1592	5.68	6.18
100	0.9368	0.288744	0.1658	5.667	6.167
200	0.988979	0.290172	0.1692	5.663	6.163
300	1.001174	0.290889	0.1693	5.662	6.162

Table 2. Test cases for the dimensionless model

	Q	N	Pe	H	ζ
Case 1	$1*10^4$	0.1	$1*10^3$	10^4	10^3
Case 2	$1*10^4$	1	10^4	10^4	10^3
Case 3	$5*10^4$	10	$5*10^3$	10^4	10^4
Case 4	$5*10^4$	0	10^4	10^4	10^4

consecutive iterations is smaller than 10^{-8} for all the grid points in the computational domain.

Table 1 presents the results of one of our grid independent studies. We had utilized a set of $N_g = 50$, 100, 200, and 300 points in the x direction. It can be seen that the maximum error in the average Nusselt number and average temperature of fluid and solid phases is about 0.109% for a $N_g = 200$. As such, $N_g = 200$ is considered to provide grid independent results.

To further validate our results we have compared the results from our own FVM code with the results obtained using a FEM commercial code (COMSOL) [35], while both convection and radiation were included. Excellent agreement was observed for all cases shown in Table 2 and displayed in Figure 3.

4. RESULTS AND DISCUSSION

Figure 4 depicts the solid and fluid phase temperature distributions for different values of conduction-radiation parameter, N along the X direction. It can be seen, that the temperature gradient decreases for the solid phase but increases for the fluid phase when N increases from 0.1 to 10. An increase in the conduction-radiation parameter, N translates into an increase in the total conductivity of the solid phase based on the diffusion approximation. Consequently, the
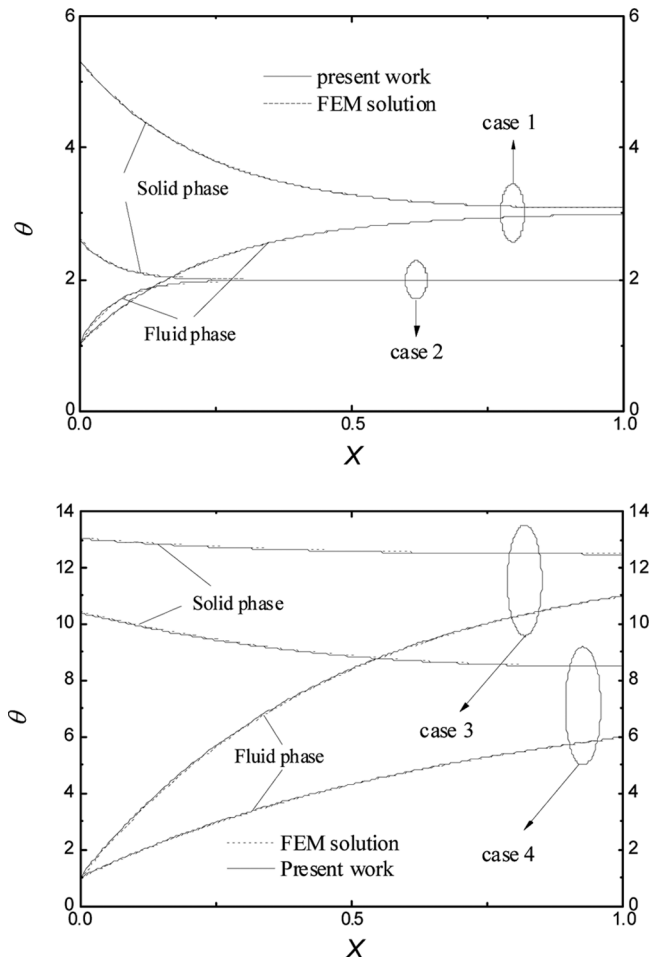
Figure 3. Comparison of numerical results between our FVM developed code and a commercial FEM code (COMSOL).

solid temperature gradient decreases as N increases. In addition, the result of a traditional LTNE model without incorporating the radiation effect is also included in Figure 4 ($N = 0$).

As expected when the Peclet number Pe and the interphase convective parameter H increase, convection increases, resulting in larger temperature gradients. The effect of the conduction-radiation parameter, N diminishes at larger values of the Pe and H, as can be seen by comparing Figures 4a and 4b.

As the ratio of solid to fluid conductivity, ζ increases, the solid temperature gradient decreases substantially. This can be seen when comparing Figures 4a and 4c. Furthermore, as expected, for larger values of Pe, H, and ζ the effect of conduction-radiation parameter N is highly diminished, as seen in Figure 4d.

Thermal efficiency is an important parameter for the high temperature air receiver, an effective way to increase the efficiency is to reduce the radiation heat loss
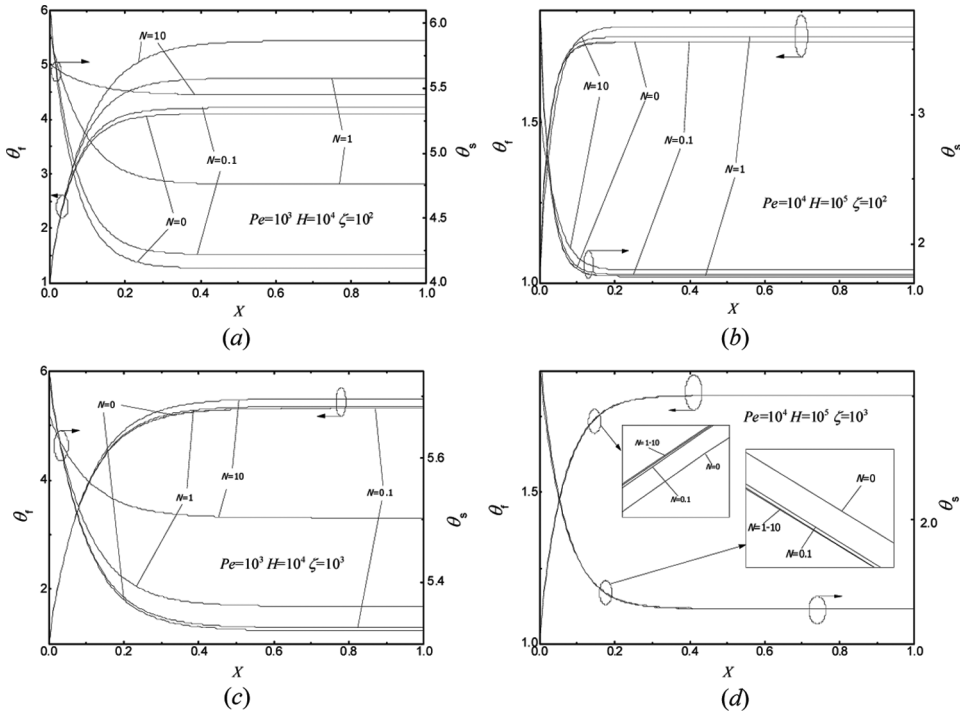
Figure 4. Effect of conduction-radiation parameter N on the temperature distribution along the flow direction: (a) $Pe = 10^3$, $H = 10^4$, $\zeta = 10^2$; (b) $Pe = 10^4$, $H = 10^5$, $\zeta = 10^2$; (c) $Pe = 10^3$, $H = 10^4$, $\zeta = 10^3$; (d) $Pe = 10^4$, $H = 10^5$, $\zeta = 10^3$.

at the surface of receiver. For example, a high transparency quartz glass structure can be used as a cover to maximize the radiation input while reducing the losses [36]. Thermodynamically, the higher the HTF outlet temperature, the higher the overall power plant performance will be. Consequently, it is worth noting from studying the presented overall temperature distributions, that the changes in the conduction-radiation parameter, N substantially influences the entrance temperature of the solid phase $\theta_{s,i}$ and the outlet temperature of the fluid $\theta_{f,o}$. To examine the significance of this trend, the contour maps for $\theta_{s,i}$ and $\theta_{f,o}$ for a wide range of H and N with a constant $Pe = 10^3$ is presented in Figure 5. It can be seen that when H is constant, $\theta_{s,i}$ decreases while $\theta_{f,o}$ increases with an increase in N, leading to an improvement in the thermal efficiency. This trend becomes more apparent for lower values of ζ, as can be seen in Figures 5b and 5d. Our results show that decreasing the extinction coefficient of the porous matrix without changing the other properties will improve the thermal performance of the air receiver.

The local Nusselt numbers, Nu_l for both phases are defined as follows.

$$Nu_f = \frac{L}{\theta_{m_f} - \theta_e} \frac{d\theta_f}{dX} \tag{23}$$
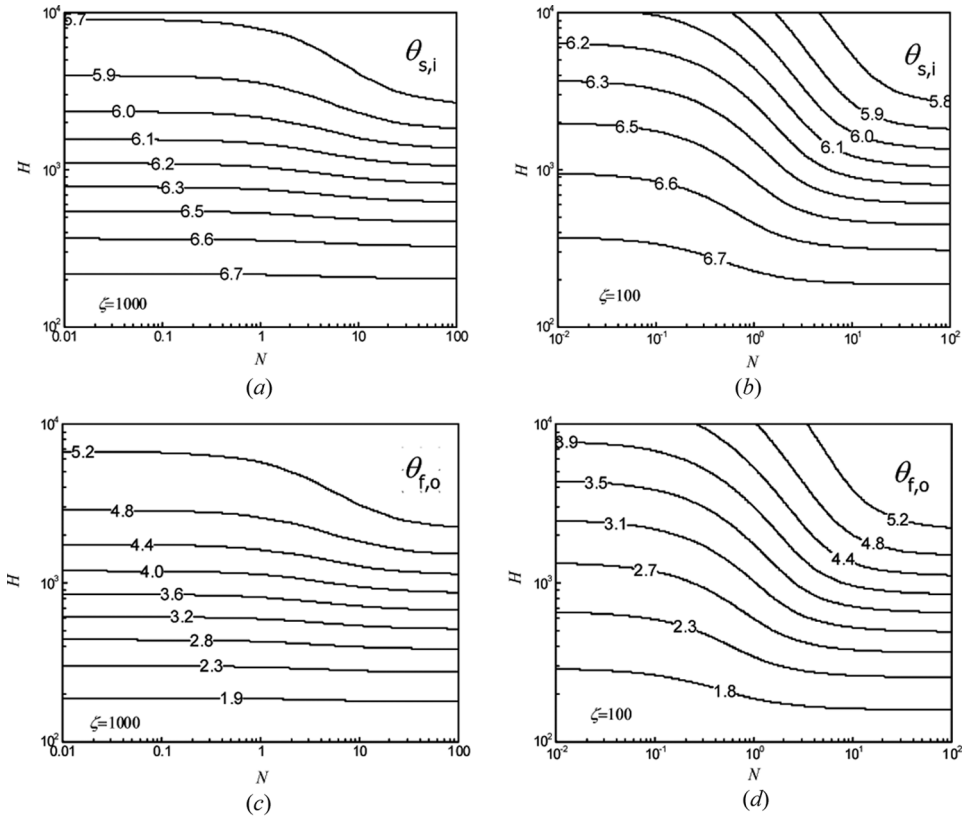
Figure 5. Effect of interphase convection parameter H and conduction–radiation parameter, N on (a), (b) the entrance temperature of the solid phase, $\theta_{s,i}$; (c), (d) the outlet temperature of the fluid phase $\theta_{f,o}$.

$$\text{Nu}_{sr} = \frac{RL}{\theta_{m_s} - \theta_e} \frac{d\theta_s}{dX} \tag{24}$$

$$\text{Nu}_{sc} = \frac{(1-R)L}{\theta_{m_s} - \theta_e} \frac{d\theta_s}{dX} \tag{25}$$

where R is defined as follows.

$$R = \frac{N\theta_s^3}{N\theta_s^3 + \zeta} \tag{26}$$

θ_{ms}, θ_{mf} are the average temperature values along the X direction and are defined as follows.

$$\theta_{m_f} = \frac{\int_0^{X_L} \theta_f dX}{X_L} \tag{27}$$

$$\theta_{m_s} = \frac{\int_0^{X_L} \theta_s dX}{X_L} \tag{28}$$

It should be noted that Nu_f represents the effect of convection between two phases; however, Nu_{sr} and Nu_{sc} express the conduction and radiation in the X direction in the solid phase, respectively. The effect of conduction-radiation parameter N on the local Nusselt number is shown in Figure 6. It can be seen that Nu_f, Nu_{sc}, and Nu_{sr} all decrease along the X direction, and that Nu_{sc} decreases and Nu_{sr} increases
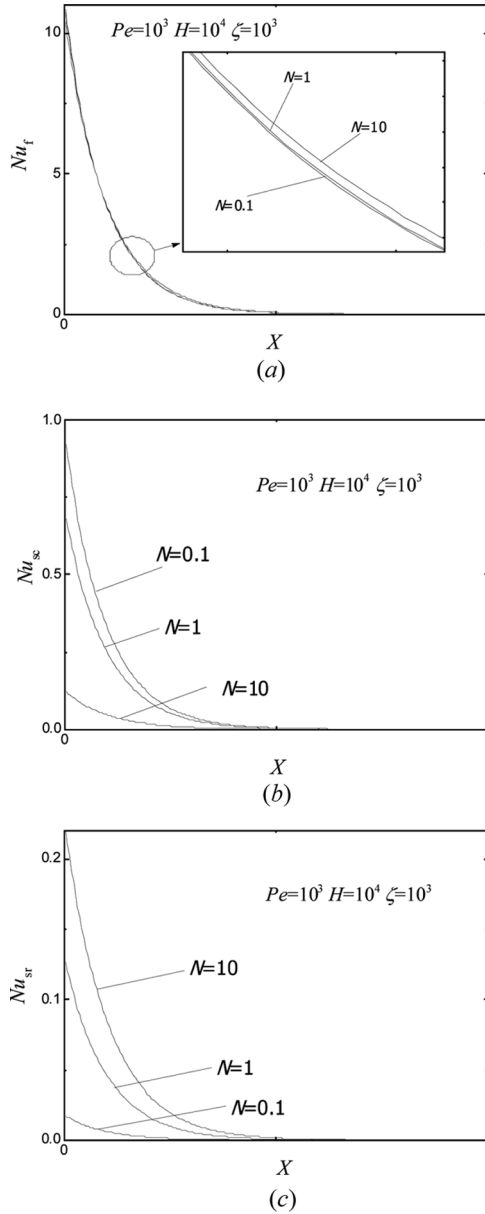
Figure 6. Effect of conduction-radiation parameter N on (a) Nu_f, (b) Nu_{sc}, (c) Nu_{sr} for $Pe = 10^3$, $H = 10^4$, and $\zeta = 10^3$.

sharply as N increases, while the change of Nu_f is relatively minor. The effect of ratio of solid to fluid conductivities, ζ on Nu_f, Nu_{sc}, and Nu_{sr} is shown in Figure 7 for $Pe = 10^3$, $H = 10^4$, and $N = 1$. As it can be seen, variations in ζ have a minimal effect on Nu_f, while Nu_{sc} increases and Nu_{sr} decreases sharply as ζ increases. Generally, the
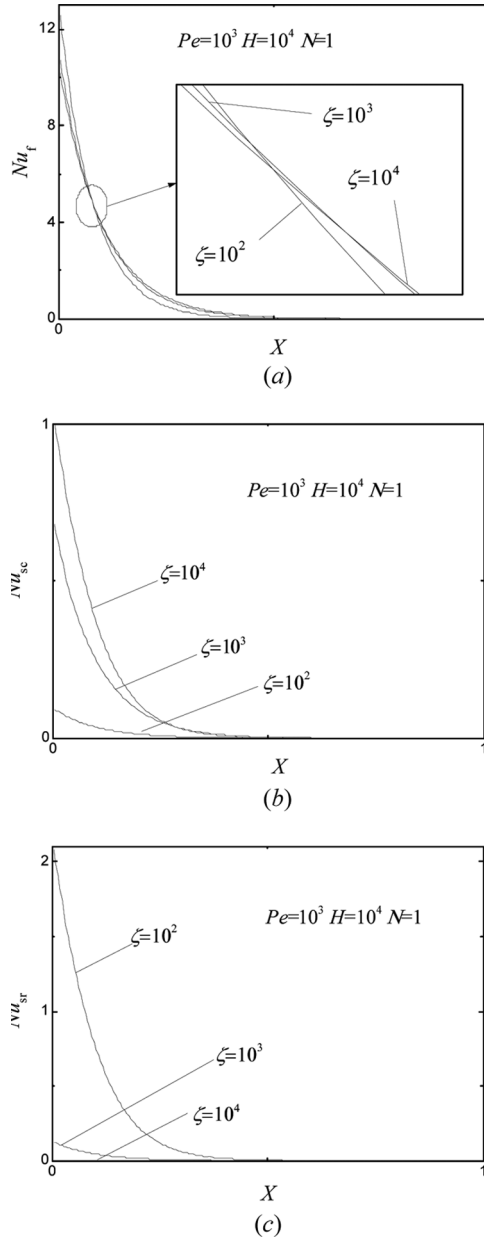
Figure 7. Effect of solid to fluid conductivity ratio ζ on (a) Nu_f, (b) Nu_{sc}, (c) Nu_{sr} for $Pe = 10^3$, $H = 10^4$, $\zeta = 10^3$, and $N = 1$.

limiting interactions between conduction and radiation incorporating convection can be observed from Figures 4–7.

To gain additional insight with respect to the impact of the radiation on the overall energy transport we introduce R_r, the ratio of $\mathrm{Nu}_{r,a}$ to the summation of $\mathrm{Nu}_{c,a}$ and $\mathrm{Nu}_{r,a}$, as follows.

$$R_r = \frac{\mathrm{Nu}_{r,a}}{\mathrm{Nu}_{r,a} + \mathrm{Nu}_{c,a}} \tag{29}$$

Where the average Nusselt numbers $\mathrm{Nu}_{r,a}$ and $\mathrm{Nu}_{c,a}$ over the thickness of the receiver are expressed as follows.

$$\mathrm{Nu}_{r,a} = \frac{\int_{X_L} \mathrm{Nu}_{sr} dX}{X_L} \tag{30}$$
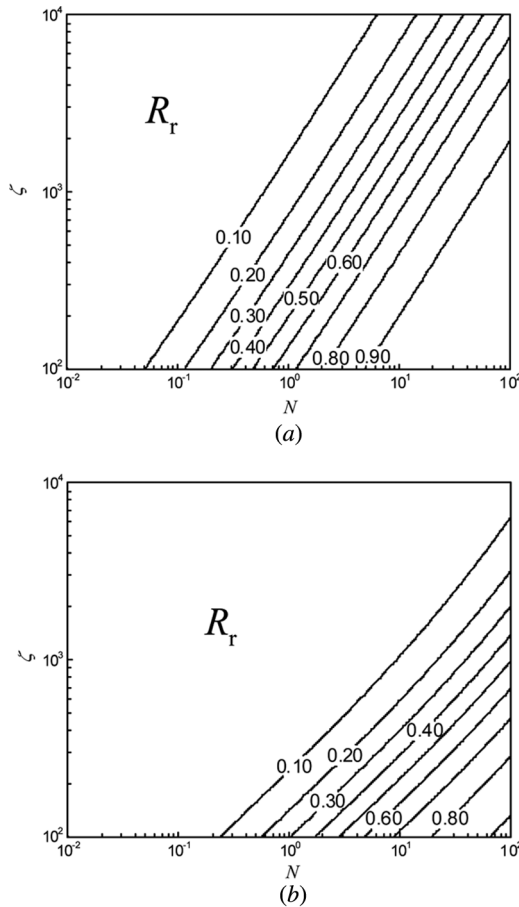
Figure 8. Effect of the solid to fluid conductivity ratio ζ and conduction-radiation parameter N on R_r for (a) $\mathrm{Pe} = 10^3$ and $H = 10^4$, and (b) $\mathrm{Pe} = 10^4$, and $H = 10^5$.

$$\mathrm{Nu}_{c,a} = \frac{\int_{X_L} \mathrm{Nu}_{sc} dX}{X_L} \tag{31}$$

It should be noted, that R_r represents the average percentage of energy transported by thermal radiation, the variation of R_r as a function of N and ζ is displayed in Figure 8. As can be seen, R_r increases with an increase in N, but it decreases with an increase in ζ. An increase in convection results in a relatively lower value of R_r, as can be seen in Figure 8b.

The effect of variations in N and ζ on $\mathrm{Nu}_{c,a}$, $\mathrm{Nu}_{r,a}$ is shown in Figure 9. As it can be seen $\mathrm{Nu}_{c,a}$ decreases with an increase in N at a constant value of ζ; however, it first increases and then decreases with an increase in ζ at a constant N. Likewise, $\mathrm{Nu}_{r,a}$ decreases with an increase in ζ when N is constant, but it first increases and then decreases with an increase of N at a constant ζ. Generally, the impact of N
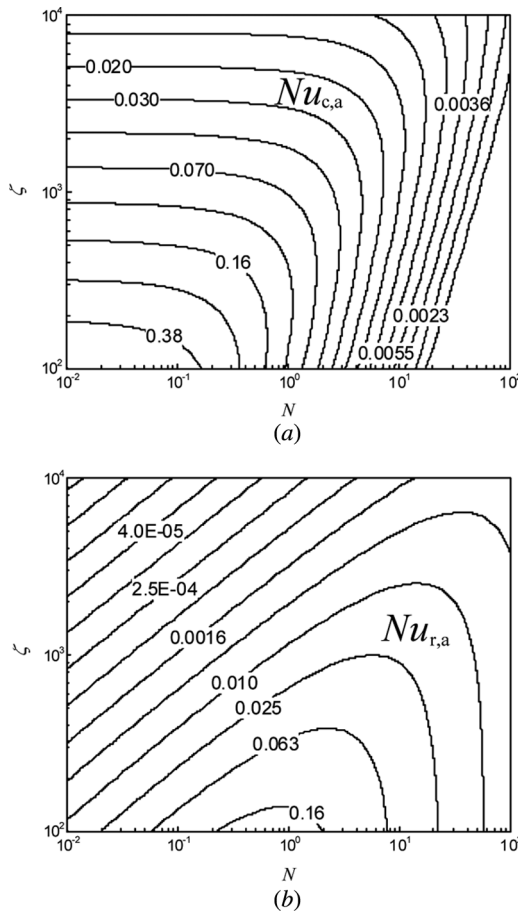
Figure 9. Effect of variation in conduction-radiation parameter N and solid to fluid conductivity ratio ζ on (a) $\mathrm{Nu}_{c,a}$, and (b) $\mathrm{Nu}_{r,a}$ for $\mathrm{Pe} = 10^3$ and $H = 10^4$.

on $\mathrm{Nu}_{c,a}$ and that of ζ on $\mathrm{Nu}_{r,a}$ is monotonic. In contrast, the impact of N on $\mathrm{Nu}_{r,a}$ and that of ζ on $\mathrm{Nu}_{c,a}$ is non-monotonic. The reason for this behavior can be traced to Eqs. (24)–(31); that is, an increase in N results in an increase in R, while the temperature gradient decreases simultaneously, consequently, leading to the creation of a maxima. That is, the radiation heat flux has a peak value within the range of variations of the conduction-radiation parameter N.

The contour maps for $\mathrm{Nu}_{c,a}$, $\mathrm{Nu}_{r,a}$ distributions in terms of parameters H and N are displayed in Figure 10. It is interesting to note that an extreme value appears again when H increases at constant value of N. This phenomenon is based on the non-monotonic effect of H on the temperature gradient; that is, as the strength of convection increases, the rate of change of the temperature in front of the solid phase is slow at first and then it becomes faster, however for the lower temperature area at the end, the rate of change is fast at first and then it slows down. As a result, the temperature gradient in the X direction increases at first and then it decreases. This
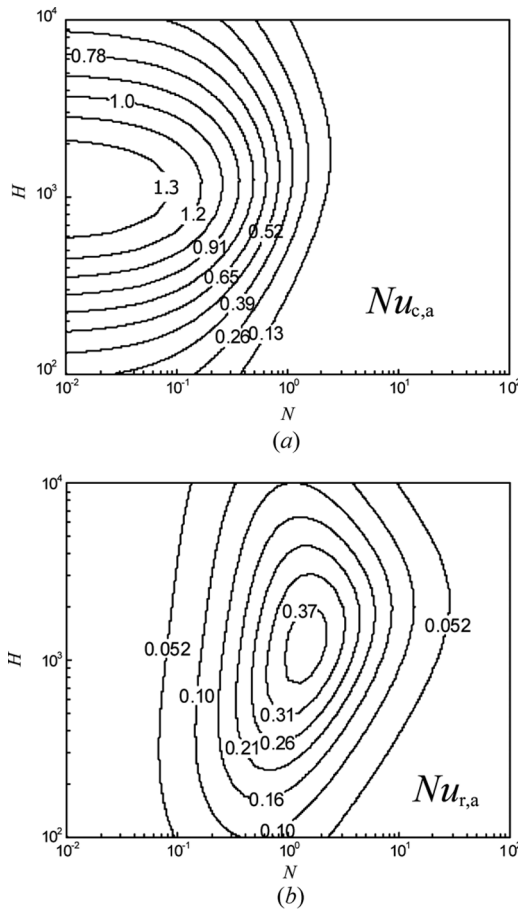
Figure 10. Effect of interphase convection parameter H and conduction-radiation parameter N on (a) $\mathrm{Nu}_{c,a}$ and (b) $\mathrm{Nu}_{r,a}$ for $\mathrm{Pe} = 10^3$ and $\zeta = 10^2$.

result affirms the presence of an extreme for the thermal radiative and conductive energy transport in the presence of convection.

5. CONCLUSION

The effect of thermal radiation in a porous medium in the presence of local thermal nonequilibrium convection for a solar air receiver is analyzed in this work. The following conclusions can be drawn based on our analysis.

1. The temperature gradient decreases for the solid phase and increases for the fluid phase with an increase in the conduction-radiation parameters N from 0.1 to 10. An increase in conduction decreases the temperature gradient of the solid phase while an increase in convection decreases it.
2. The conduction-radiation parameter N substantially affects the entrance temperature of the solid phase $\theta_{s,i}$ and outlet temperature of the fluid $\theta_{f,o}$. $\theta_{s,i}$ decreases and $\theta_{f,o}$ increases with an increase in N at a constant value of H.
3. Variations in N and ζ have a negligible effect on Nu_f, while its effect on Nu_{sc} and Nu_{sr} are in the opposite directions. R_r which represents the average percentage of energy transported by thermal radiation increases with an increase in N, while it decreases with an increase in ζ. An increase in convection results in a relatively lower value of R_r.
4. An increase in the conduction-radiation parameter N results in an increase in R, while the temperature gradient decreases. As such $\mathrm{Nu}_{r,a}$ possess a maxima point. That is the radiation heat flux has a peak at a corresponding value of N. When considering the effect of ζ on $\mathrm{Nu}_{c,a}$, a similar mechanism is established.
5. A maximum point also appears as H increases at a constant value of N. The reason for this phenomenon is that effect of H on temperature gradient is non-monotonic; that is, as convection increases, the rate of change of temperature for the local temperature is affected. This result confirms that there must be a maxima point for the thermal radiative and conductive energy transport at a corresponding value of H while incorporating the convective heat transfer.

FUNDING

REFERENCES

1. K. Vafai, *Handbook of Porous Media*, CRC, New York, 2000.
2. A. L. Aacutevila-Mariacuten, Volumetric Receivers in Solar Thermal Power Plants with Central Receiver System Technology: A Review, *Solar Energy*, vol. 85, no. 5, pp. 891–910910, 2011.

3. K. Vafai and C. L. Tien, Boundry and Inertial Effects on Flow and Heat Transfer in Porous Media, *Int. J. of Heat and Mass Transfer*, vol. 24, pp. 195–203, 1981.

4. K. Vafai, Convective Flow and Heat Transfer in Variable-Porosity Media, *J. of Fluid Mechanics*, vol. 147, pp. 233–259, 1984.

5. K. Vafai and M. Sozen, Analysis of Energy and Momentum Transport for Fluid Flow through a Porous Bed, *J. of Heat Transfer*, vol. 112, no. 3, pp. 690–699, 1999.

6. A. Amiri and K. Vafai, Analysis of Dispersion Effects, and Local Thermal Nonequilibrium, Uon-Darcean, Variable Porosity Incompressible Flow through Porous Media, *Int. J. of Heat and Mass Transfer*, vol. 37, no. 6, pp. 939–954, 1994.

7. A. Amiri and K. Vafai, Transient Analysis of Incompressible Flow through a Packed Bed, *Int. J. of Heat and Mass Transfer*, vol. 41, no. 24, pp. 4259–4279, 1998.

8. B. Alazmi and K. Vafai, Analysis of Variants Within the Porous Media Transport Models, *J. of Heat Transfer*, vol. 122, pp. 303–326, 2000.

9. K. Yang and K. Vafai, Analysis of Temperature Gradient Bifurcation in Porous Media—An Exact Solution, *Int. J. of Heat and Mass Transfer*, vol. 53, no. 19–20, pp. 4316–4325, 2010.

10. K. Yang and K. Vafai, Analysis of Heat Flux Bifurcation Inside Porous Media Incorporating Inertial and Dispersion Effects—An Exact Solution, *Int. J. of Heat and Mass Transfer*, vol. 54, no. 25–26, pp. 5286–5297, 2011.

11. B. Alazmi and K. Vafai, Constant Wall Heat Flux Boundary Conditions in Porous Media Under Local Thermal Non-Equilibrium Conditions, *Int. J. of Heat and Mass Transfer*, vol. 45, pp. 3071–3087, 2002.

12. C. L. Tien, Thermal-Radiation in Packed and Fluidized-Beds, *J. Heat Transfer—Trans Asme*, vol. 110, no. 4B, pp. 1230–1242, 1988.

13. C. L. Tien and K. Vafai, Convective and Radiative Heat Transfer in Posous Dedia, *Adv. in Applied Mechanics*, vol. 27, pp. 225–281, 1990.

14. K. Vafai and J. Ettefagh, Analysis of the Radiative and Conductive Heat Transfer Characteristics of a Waste Package Canister, *ASME J. of Heat Transfer*, vol. 110, pp. 1011–1014, 1988.

15. B. P. Singh and M. Kaviany, Independent Theory Versus Direct Simulation of Radiation Heat Transfer in Packed Beds, *Int. J. of Heat and Mass Transfer*, vol. 34, no. 11, pp. 2869–2882, 1991.

16. B. P. Singh and M. Kaviany, Modelling Radiative Heat Transfer in Packed Beds, *Int. J. of Heat and Mass Transfer*, vol. 35, no. 6, pp. 1397–1405, 1992.

17. C. Y. Zhao, T. J. Lu, and H. P. Hodson, Thermal Radiation in Ultralight Metal Foams with Open Cells, *Int. J. of Heat and Mass Transfer*, vol. 47, no. 14–16, pp. 2927–2939, 2004.

18. C. Y. Zhao, S. A. Tassou, and T. J. Lu, Analytical Considerations of Thermal Radiation in Cellular Metal Foams with Open Cells, *Int. J. of Heat and Mass Transfer*, vol. 51, no. 3–4, pp. 929–940, 2008.

19. T. J. Hendricks and J. R. Howell, New Radiative Analysis Approach for Reticulated Porous Ceramics using Discrete Ordinates Method, *J. of Heat Transfer*, vol. 118, no. 4, pp. 911–917, 1996.

20. T. J. Hendricks and J. R. Howell, Absorption/Scattering Coefficients and Scattering Phase Functions in Reticulated Porous Ceramics, *J. of Heat Transfer*, vol. 118, no. 1, pp. 79–87, 1996.

21. D. Baillis, M. Raynaud, and J. F. Sacadura, Spectral Radiative Properties of Open-Cell Foam Insulation, *J. Thermophy. Heat Transfer*, vol. 13, no. 3, pp. 292–298, 1999.

22. D. Baillis and J.-F. Sacadura, Thermal Radiation Properties of Dispersed Media: Theoretical Prediction and Experimental Characterization, *J. of Quantitative Spectroscopy and Radiative Transfer*, vol. 67, no. 5, pp. 327–363, 2000.

23. F. Bai, One Dimensional Thermal Analysis of Silicon Carbide Ceramic Foam used for Solar Air Receiver, *Int. J. of Thermal Sciences*, vol. 49, no. 12, pp. 2400–2404, 2010.
24. C. Xu, Z. Song, L.-D. Chen, and Y. Zhen, Numerical Investigation on Porous Media Heat Transfer in a Solar Tower Receiver, *Renewable Energy*, vol. 36, no. 3, pp. 1138–1144, 2011.
25. Z. Y. Wu, C. Caliot, G. Flamant, and Z. F. Wang, Coupled Radiation and Flow Modeling in Ceramic Foam Volumetric Solar Air Receivers, *Solar Energy*, vol. 85, no. 9, pp. 2374–2385, 2011.
26. B. Hoffschmidt, F. L. M. Téllez, A. Valverde, J. S. Fernández, and V. Fernández, Performance Evaluation of the 200-kWth HiTRec—II Open Volumetric Air Receiver, *J. Sol. Energy Eng.*, vol. 125, no. 1, pp. 87–94, 2003.
27. M. Becker, T. Fend, B. Hoffschmidt, R. Pitz-Paal, O. Reutter, V. Stamatov, M. Steven, and D. Trimis, Theoretical and Numerical Investigation of Flow Stability in Porous Materials Applied as Volumetric Solar Receivers, *Solar Energy*, vol. 80, no. 10, pp. 1241–1248, 2006.
28. R. Pitz-Paal, B. Hoffschmidt, M. Böhmer, and M. Becker, Experimental and Numerical Evaluation of the Performance and Flow Stability of Different Types of Open Volumetric Absorbers Under Non-Homogeneous Irradiation, *Solar Energy*, vol. 60, no. 3–4, pp. 135–150, 1997.
29. T. Fend, B. Hoffschmidt, R. Pitz-Paal, O. Reutter, and P. Rietbrock, Porous Materials as Open Volumetric Solar Receivers: Experimental Determination of Thermophysical and Heat Transfer Properties, *Energy*, vol. 29, no. 5–6, pp. 823–833, 2004.
30. T. Fend, R. Pitz-Paal, O. Reutter, J. Bauer, and B. Hoffschmidt, Two Novel High-Porosity Materials as Volumetric Receivers for Concentrated Solar Radiation, *Solar Energy Materials and Solar Cells*, vol. 84, no. 1–4, pp. 291–304, 2004.
31. J. R. Howell, R. Siegel and M. P. Mengüç, *Thermal Radiation Heat Transfer*, 5th ed., CRC Press, Boca Raton, FL, 2011.
32. M. E. Goldstein and J. R. Howell, Boundary Conditions for the Diffusion Solution of Coupled Conduction-Radiation Problems, Technical Note, *NASA*, 1968.
33. M. E. Larsen, Use of Contact Resistance Algorithm to Implement Jump Boundary Coonditions for the Radiation Diffusion Approximation, Sandia National Lab. Rept. SAND2005-1482C, Albuquerque, New Mexico, 2005.
34. W. Q. Tao, *Numerical Heat Transfer*, 2nd ed., Xi'an Jiaotong University Press, Xi'an, P. R. China, 2001.
35. Comsol, COMSOL Multiphysics User's Guide, 2010.
36. R. Pitz-Paal, J. Morhenne, and M. Fiebig, A New Concept of a Selective Solar Receiver for High Temperature Applications, *Solar Energy Materials*, vol. 24, no. 1–4, pp. 293–306, 1991.